15 DIGITAL PROCESSING OF DIFFUSION-TENSOR IMAGES OF AVASCULAR TISSUES

Konstantin I. Momot, James M. Pope and R. Mark Wellard

CONTENTS

15.1 Introduction

Diffusion is the process that leads to the mixing of substances as a result of spontaneous and random thermal motion of individual atoms and molecules. It was first detected by the English botanist Robert Brown in 1827, and the phenomenon became known as 'Brownian motion'. More specifically, the motion observed by Brown was *translational diffusion* – thermal motion resulting in random variations of the position of a molecule. This type of motion was given a correct theoretical interpretation in 1905 by Albert Einstein, who derived the relationship between temperature, the viscosity of the medium, the size of the diffusing molecule, and its *diffusion coefficient* (1). It is translational diffusion that is indirectly observed in MR diffusion-tensor imaging (DTI). The relationship obtained by Einstein provides the physical basis for using translational diffusion to probe the microscopic environment surrounding the molecule.

In living systems translational diffusion is vital for the transport of water and metabolites both into and around cells. In the presence of a *concentration gradient*, diffusion results in the mixing of substances: The molecules of a compound on average tend to move from areas of high concentration into areas of low concentration, resulting in a net transport of the compound in the direction of the gradient. A classic example of this is the spontaneous mixing of a dyestuff into a stationary solvent.
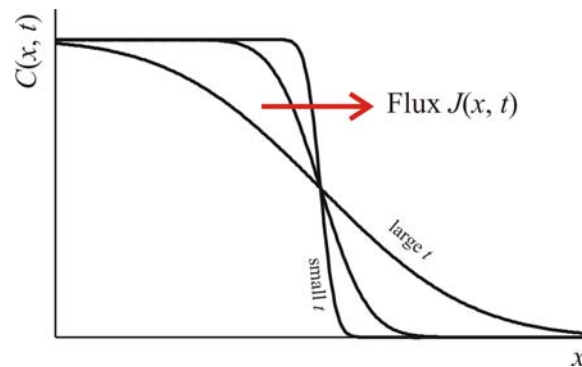
Figure 15.1 Diffusion in the presence of a concentration gradient $C(x, t)$, gives rise to a net flux or flow of particles $J(x, t)$ from high to low concentration.

Diffusive mass transport can serve as the basis for the measurement of molecular diffusion: a concentration gradient is artificially created, and its equilibration with time observed. This method of measuring diffusion is not always physically relevant because a concentration gradient is neither required for diffusion nor always present. The majority of DTI applications are based on the diffusion of water, whose concentration is essentially uniform in extracellular and intracellular microenvironments of living organisms. Diffusion of molecules of the same substance in the absence of a concentration gradient is known as '*self-diffusion*'. It is self-diffusion that is observed in DTI. Self-diffusion can be measured by the technique of Pulsed Field Gradient Nuclear Magnetic Resonance (PFG-NMR), which is exquisitely sensitive to the microstructural environment of nuclear spins. (Other examples of applications of magnetic resonance to tissues can be seen in

Chapters 5, 9 and 10.) In recent years, PFG-NMR has been increasingly combined with Magnetic Resonance Imaging (MRI) to study diffusion of water protons in biological tissues for diagnosis of stroke and multiple sclerosis, for white matter fibre tracking in the brain, muscle fibre tracking and other applications.

While no concentration gradient is necessary for DTI, the notion of a concentration gradient is instructive for understanding how DTI works. In an isotropic medium such as bulk water, the process of diffusion is itself isotropic and can be described by a scalar diffusion coefficient D. If we were to "label" a subset of molecules, the flux of the labelled molecules would be governed by Fick's first law of diffusion:

$$\mathbf{J}(\mathbf{r},t) = -D\,\nabla C(\mathbf{r},t) \equiv -D\left(\mathbf{i}\frac{\partial C}{\partial x} + \mathbf{j}\frac{\partial C}{\partial y} + \mathbf{k}\frac{\partial C}{\partial z}\right) \qquad (15.1)$$

Here, $C(\mathbf{r}, t)$ is the spatial concentration profile of the labelled molecules; D is the diffusion coefficient; and $\mathbf{J}$ is the flux of particles, defined as the amount of substance that flows through a unit area per unit time. The meaning of Eq. (15.1) is that in isotropic media the flux occurs strictly in the direction of the concentration gradient. Combining Eq. (15.1) with the conservation of mass and the assumption that D is independent of concentration yields Fick's second law of diffusion or the diffusion equation:

$$\frac{\partial C(\mathbf{r},t)}{\partial t} = D\,\nabla^2 C(\mathbf{r},t) \equiv D\left(\frac{\partial^2 C}{\partial x^2} + \frac{\partial^2 C}{\partial y^2} + \frac{\partial^2 C}{\partial z^2}\right) \qquad (15.2)$$

Diffusion in biological tissues is substantially different from isotropic diffusion. Tissues are intrinsically heterogeneous: there are barriers to free diffusion of water molecules arising from the presence of macromolecules, organelles, cell membranes and larger scale structures. As a result, diffusion of water molecules in many tissues is both *restricted* and *anisotropic*.

Restricted diffusion results in measurements of the diffusion coefficient giving results that are dependent on the *time-scale* of the diffusion interval Δ over which the measurement is performed. This is known as an 'apparent diffusion coefficient' (ADC). Besides Δ, the ADC is dependent on the nature and the length scale of the obstructions and is generally smaller than the self-diffusion coefficient of bulk water ($D_0 = 2.3 \cdot 10^{-9}$ m^2 s^{-1} at 25 $^{\circ}$C). For example, the ADC of water confined between parallel, semi-permeable barriers approximately equals D_0 at $\Delta << d^2/D_0$, where d is the separation between the barriers, but decreases to $D_0/(1+1/P)$ at $\Delta >> d^2/D_0$ (where P is the permeability of the barriers) (2).

Anisotropic diffusion means that the diffusing molecules encounter *less restriction in some directions than others*. Diffusion can be anisotropic when the tissue possesses some form of global alignment. Two well-known examples of anisotropic tissues are the white matter of the brain and the heart muscle. In muscles, the global alignment arises from the elongated form of the muscle cells forming muscle fibres. In white matter, the anisotropy arises from the fact that nerve fibre tracts follow specific pathways. In both these cases, the cellular

structures preferentially restrict the diffusion of water in the direction perpendicular to the fibres. Diffusion is also anisotropic in the two tissues that are the focus of this Chapter: articular cartilage (AC) and the eye lens. In AC, the anisotropic restrictions to diffusion are imposed by the aligned collagen fibres that form the biomacromolecular "scaffold" of the tissue. In the crystalline eye lens, the restrictions are imposed by the fibre cells.

To take account of anisotropic diffusion, a common approach is to re-write the diffusion equation in terms of a *diffusion tensor*:

$$\mathbf{J}(\mathbf{r},t) = -\mathbf{D} \cdot \nabla C(\mathbf{r},t) \qquad (15.3)$$

where the diffusion tensor $\mathbf{D}$ is represented by a symmetric and real 3 x 3 matrix:

$$\mathbf{D} = \begin{pmatrix} D_{xx} & D_{xy} & D_{xz} \\ D_{xy} & D_{yy} & D_{yz} \\ D_{xz} & D_{yz} & D_{zz} \end{pmatrix} \qquad (15.4)$$

In the anisotropic case, Fick's second law becomes:

$$\frac{\partial C}{\partial t} = \nabla \cdot \mathbf{D} \cdot \nabla C \equiv \begin{pmatrix} \dfrac{\partial}{\partial x} & \dfrac{\partial}{\partial y} & \dfrac{\partial}{\partial z} \end{pmatrix} \begin{pmatrix} D_{xx} & D_{xy} & D_{xz} \\ D_{xy} & D_{yy} & D_{yz} \\ D_{xz} & D_{yz} & D_{zz} \end{pmatrix} \begin{pmatrix} \partial/\partial x \\ \partial/\partial y \\ \partial/\partial z \end{pmatrix} C \quad (15.5)$$

Note that while the diagonal elements of the diffusion tensor scale

concentration gradients and fluxes that are in the same direction, the off-diagonal elements couple fluxes and concentration gradients in orthogonal directions. This is because in the anisotropic case the distribution of diffusional displacements of molecules tends to follow the geometry of the restricting barriers. This is the physical basis for using DTI to measure the microscopic morphology of the tissue. In Sections 15.2.4 and 15.4, we discuss applications of DTI to the eye lens and articular cartilage, respectively, as examples.

A convenient way of representing the diffusion tensor is the diffusion ellipsoid, which is illustrated in Fig. 15.2. The shape of the ellipsoid represents the directional asymmetry of the average displacements of the diffusing molecules. The directions of the principal axes of the ellipsoid characterise the orientation of the diffusion tensor, which in turn represents the spatial anisotropy of the restricting barriers imposed by the tissue.
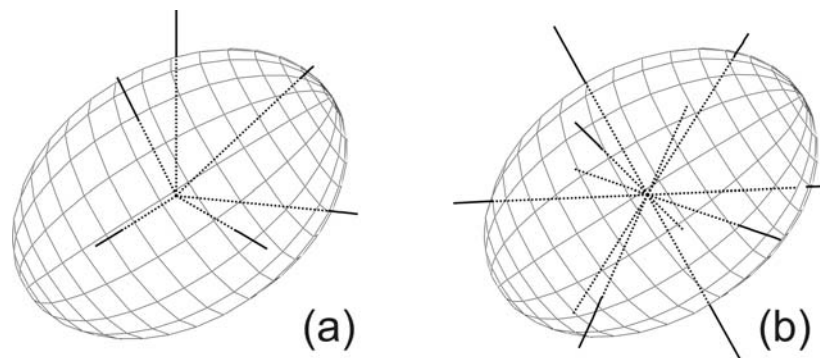

Figure 15.2 Diffusion ellipsoid as a visual representation of the diffusion tensor. The straight lines radiating from the centre of the ellipsoid illustrate two possible choices of the diffusion sampling directions, as discussed in Section 15.2.2.

In the isotropic case, the diffusion tensor is a diagonal matrix:

$$\mathbf{D} = \begin{pmatrix} D & 0 & 0 \\ 0 & D & 0 \\ 0 & 0 & D \end{pmatrix} \qquad (15.6)$$

where D is the isotropic diffusion coefficient. In this case, Eq. (15.5) reverts to Eq. (15.2), and the ellipsoid in Fig. 15.2 becomes a sphere.

15.2 Acquisition of diffusion-tensor images

15.2.1 Fundamentals of Diffusion Tensor Imaging (DTI)

Diffusion-tensor (DT) images can be obtained using Nuclear Magnetic Resonance (NMR). NMR measures the frequency of precession of nuclear spins such as that of the proton (^{1}H), which in a magnetic field $\mathbf{B}_0$, is given by the Larmor equation:

$$\omega_0 = \gamma B_0 \qquad (15.7)$$

The key to achieving spatial resolution in MRI is the application of time dependent magnetic field gradients that are superimposed on the (ideally uniform) static magnetic field $\mathbf{B}_0$. In practice the gradients are applied via a set of dedicated 3-axis gradient coils, each of which is capable of applying a gradient in one of the orthogonal directions (x, y, and z). Thus in the presence of a magnetic field gradient $\mathbf{g}$,

$$\mathbf{g} = \left(\frac{\partial B_z}{\partial x}, \quad \frac{\partial B_z}{\partial y}, \quad \frac{\partial B_z}{\partial z} \right) \qquad (15.8)$$

the magnetic field strength and hence the precession frequency become position-dependent. The strength of the magnetic field experienced by a spin at position **r** is given by:

$$B = B_0 + \mathbf{g} \cdot \mathbf{r} \qquad\qquad (15.9)$$

The corresponding Larmor precession frequency is changed by the contribution from the gradient:

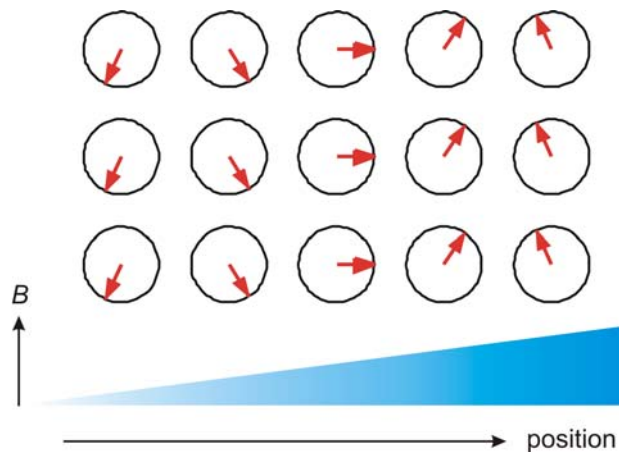$$\omega(\mathbf{r}) = \frac{\partial \phi(\mathbf{r})}{\partial t} = \gamma(B_0 + \mathbf{g} \cdot \mathbf{r}) \qquad\qquad (15.10)$$

Figure 15.3 The effect of a magnetic field gradient on precession of spins. A constant magnetic field gradient **g** (illustrated by the blue ramp) applied in some arbitrary direction changes the magnetic field at position **r** from **B**$_0$ to a new value **B** = **B**$_0$ + **g·r**. The gradient perturbs the precession of the spins, giving rise to an additional position-dependent phase ϕ', which may be positive or negative depending on whether the magnetic field produced by the gradient coils strengthens or weakens the static magnetic field B_0.

The precession frequency ω is the rate of change of the *phase*, φ, of a spin − i.e., its precession angle in the transverse plane. Therefore, the time-dependent phase φ is the integral of the precession frequency over time. In MRI we switch gradients on and off in different directions to provide spatial resolution, so the gradients are *time dependent* and the phase of a spin is given by:

$$\phi(\mathbf{r},t) = \int_0^t \omega(\mathbf{r},t')\,dt' = \gamma B_0 t + \gamma \int_0^t \mathbf{g}(t') \cdot \mathbf{r}\,dt' \qquad (15.11)$$

We observe the phase relative to the reference frequency given by Eq. (15.7). For example if the gradient is applied in the x direction in the form of a rectangular pulse of amplitude g_x and duration δ the additional phase produced by the gradients is

$$\phi'(\mathbf{r},t) = \gamma \int_0^\delta g_x(t')x\,dt' = \gamma \delta\, g_x x = 2\pi k_x x \qquad (15.12)$$

where the "spatial frequency" $k_x = \gamma \delta g_x / 2\pi$ is also known as the "k value". It plays an important role in the description of spatial encoding in MRI and can be thought of as the frequency of spatial harmonic functions used to encode the image.

In MRI to achieve spatial resolution in the plane of the selected slice (x, y) we apply gradients in both x and y directions sequentially. The NMR signal is then sampled for a range of values of the corresponding spatial frequencies k_x and k_y.

For one of these gradients (g_x say) this is achieved by keeping the amplitude fixed and incrementing the time t at which the signal is

recorded (the process called 'frequency encoding').

In the case of the orthogonal gradient (g_y) the amplitude of the gradient is stepped through an appropriate series of values. For this gradient the appropriate spatial frequency can be written:

$$k_y = \gamma \int_0^\delta g_y(t')\,dt' = \gamma \delta g_y / 2\pi \qquad (15.13)$$

The MR image is then generated from the resulting two-dimensional data set $S(k_x, k_y)$ by Fourier transformation:

$$S(x, y) = \iint S(k_x, k_y)\, e^{-2\pi i (k_x x + k_y y)}\, dk_x dk_y \qquad (15.14)$$

The Fourier transform relationship between an MR image and the raw NMR data is analogous to that between an object and its diffraction pattern.

15.2.2 The Pulsed Field Gradient Spin Echo (PFGSE) Method

Consider the effect of a gradient pair consisting of two consecutive gradient pulses of opposite sign shown in Fig. 15.4 (or alternatively two pulses of the same sign separated by the 180º RF pulse in a 'spin echo' sequence).

It is easy to show that spins moving with velocity **v** acquire a net phase shift (relative to stationary spins) that is *independent of their starting location* and given by:

$$\phi(\mathbf{v}) = -\gamma \mathbf{g} \cdot \mathbf{v} \delta \Delta \qquad (15.15)$$

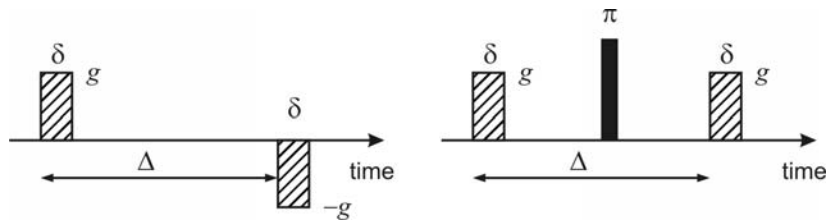where δ is the duration of each gradient in the pair and Δ is the se-

Figure 15.4 Gradient pulse pairs used for diffusion attenuation. The first gradient sensitises the magnetisation of the sample to diffusional displacement by winding a magnetisation helix. The second gradient rewinds the helix and thus enables the measurement of the diffusion-attenuated signal. The two gradients must have the same amplitude if they are accompanied by the refocusing RF π pulse; otherwise their amplitudes must be opposite.

paration of the gradients. Random motion of the spins gives rise to a *phase dispersion* and attenuation of the spin echo NMR signal.

Stejskal and Tanner (3) showed in the 1960's that, for a spin echo sequence this additional attenuation takes the form:
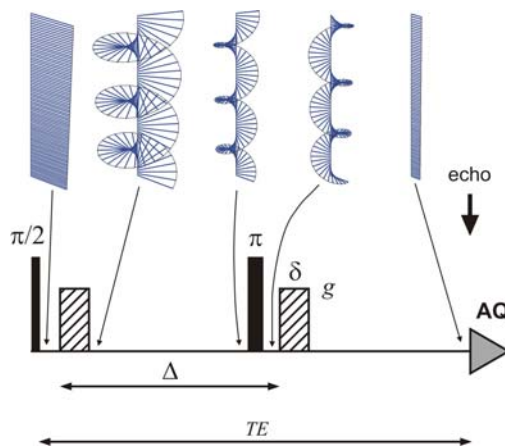

Figure 15.5 A pulsed field gradient spin echo (PGSE) sequence showing the effects of diffusive attenuation on spin echo amplitude.

$$S(\Delta, g) = S_0\, e^{-TE/T_2}\, e^{-D\gamma^2 g^2 \delta^2 (\Delta - \delta/3)} \qquad (15.16)$$

The first term is the normal echo attenuation due to transverse (spin-spin) relaxation. By stepping out the echo time TE we can measure T_2.

The second term is the diffusion term. By incrementing the amplitude of the magnetic field gradient pulses (g), we can measure the self-diffusion coefficient D.

For a fixed echo time TE we write:

$$S = S_0'\, e^{-bD} = S_0\, e^{-TE/T_2}\, e^{-bD} \qquad (15.17)$$

where

$$b = \gamma^2 g^2 \delta^2 \left(\Delta - \frac{\delta}{3} \right) \qquad (15.18)$$

The apparent diffusion coefficient (ADC) is then given by:

$$ADC = -\ln\left(\frac{S}{S_0'} \right) \Big/ b \qquad (15.19)$$

For the case of anisotropic diffusion described by a diffusion tensor **D**, the expression for the echo attenuation in a PFG spin echo experiment becomes:

$$S(\Delta, g) = S_0'\, e^{-\gamma^2 \mathbf{g} \cdot \mathbf{D} \cdot \mathbf{g}\, \delta^2 (\Delta - \delta/3)} \qquad (15.20)$$

where $\mathbf{g} = (g_x, g_y, g_z)$ is the gradient vector, and the scalar product

$\mathbf{g} \cdot \mathbf{D} \cdot \mathbf{g}$ is defined analogously to Eq. (15.5).

Overall, if diffusion is anisotropic, the echo attenuation will have an *orientation dependence* with respect to the measuring gradient $\mathbf{g}$. Gradients along the *x, y* and *z* directions sample respectively the *diagonal* elements D_{xx}, D_{yy} and D_{zz} of the diffusion tensor. In order to sample the off-diagonal elements we must apply gradients in *oblique directions* – ie combinations of g_x and g_y or g_y and g_z etc. Because the diffusion tensor is symmetric, there are just 6 independent elements. To fully determine the diffusion tensor therefore requires a minimum of 7 separate measurements – for example:

$$\begin{pmatrix} g_x \\ g_y \\ g_z \end{pmatrix} = \begin{pmatrix} 0 \\ 0 \\ 0 \end{pmatrix}, \begin{pmatrix} g \\ 0 \\ 0 \end{pmatrix}, \begin{pmatrix} 0 \\ g \\ 0 \end{pmatrix}, \begin{pmatrix} 0 \\ 0 \\ g \end{pmatrix}, \frac{1}{\sqrt{2}}\begin{pmatrix} g \\ g \\ 0 \end{pmatrix}, \frac{1}{\sqrt{2}}\begin{pmatrix} g \\ 0 \\ g \end{pmatrix}, \frac{1}{\sqrt{2}}\begin{pmatrix} 0 \\ g \\ g \end{pmatrix} \qquad (15.21)$$

This choice of diffusion gradient directions is illustrated in Fig. 15.2a. We shall refer to a data set measured with this set of gradients as the *minimal diffusion-tensor dataset*. As seen below, this is neither the only nor the best choice of DTI gradient directions. Other gradient combinations exist that achieve optimal signal-to-noise ratio (S/N) in the resulting diffusion tensor images and/or optimal gradient amplifier efficiency (see Sec. 15.2.5). The first measurement with all gradients off is required to determine S_0'.

15.2.3 Diffusion Imaging Sequences

Diffusion gradients can readily be incorporated in a conventional spin echo MRI sequence as follows:
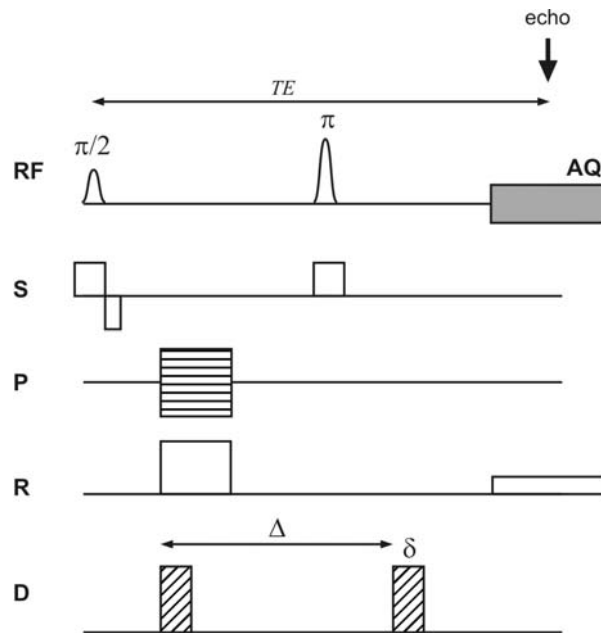
Figure 15.6 Spin echo diffusion imaging pulse sequence. "RF" denotes the RF pulses and acquisition. Gradient pulses: S, slice selection; P, encoding in the Phase direction; R, encoding in the Read direction; D, diffusion gradients.

The sequence is repeated for the appropriate different combinations of gradients g_x, g_y and g_z to yield a set of 7 different diffusion weighted images. These are then used to calculate the elements of the diffusion tensor, pixel by pixel, to yield 6 images representing the three diagonal elements and 3 off-diagonal elements of the diffusion tensor. (Because of the symmetry of the diffusion tensor the off-diagonal elements are duplicated in the 3 x 3 diffusion tensor image). Once obtained the diffusion tensor must be diagonalised to obtain the eigenvalues and eigenvectors. For more details see e.g. Basser and Jones (4).

For a given DTI imaging sequence and available MRI hardware, the effects of T_2 relaxation can be minimised by making more efficient use of available gradient power to maximise b values and reduce the minimum echo time TE. For example by ensuring that gradients are applied simultaneously along two axes at the maximum amplitude for each individual axis, the resultant gradient amplitude is increased by a factor of $\sqrt{2}$, while by employing all three basic gradients in an icosahedral arrangement it is possible to increase the maximum amplitude by Fibonacci's golden ratio: $\left(1+\sqrt{5}\right)/2$ [see e.g. reference (5) and references therein]. This choice of diffusion gradient directions is illustrated in Fig. 15.2b.

For clinical applications of DTI, patient motion can be a serious problem because even relatively small bulk motions can obscure the effects of water diffusion on the NMR signal. In such applications it is common to employ spin echo single shot echo planar imaging (SS-EPI) sequences that incorporate diffusion weighting in order to acquire an entire DWI data set in a fraction of a second, (albeit at somewhat reduced spatial resolution when compared with more conventional spin echo imaging sequences). Such SS-EPI sequences also have the added advantage of a relatively high signal to noise ratio (SNR) per unit of scanning time, allowing a complete DTI data set to be acquired in 1-2 minutes. Further improvemens in acquisition time and/or SNR can be achieved by combining such sequences with parallel imaging techniques and/or partial Fourier encoding of k-space (see e.g. (6) and references therein).

15.2.4 Example: Anisotropic Diffusion of Water in the Eye Lens

We have used the PFGSE method to measure the components of the diffusion tensor for water (H_2O) in human eye lenses (7). In this case we were measuring diffusion on a timescale of ~20ms corresponding to diffusion lengths $\ell = \sqrt{2Dt} \cong 10\mu m$ with $D = 2.3 \cdot 10^{-9}$ m^2 s^{-1} for bulk water at 20 ^{o}C and $t = 20$ ms. This is comparable to the cell dimensions. Since the cells are fibre–like in shape (ie long and thin) with diameter ~8 µm, we might expect to observe diffusion anisotropy on this timescale.

Note that four of the off-diagonal elements in the (undiagonalised) diffusion tensor are almost zero. This implies that in this example diagonalisation (see below) involves a simple rotation of axes about the normal to the image plane.

If we assume cylindrical symmetry for the cell fibres within a voxel then $\varepsilon = 0$ and in the principal axes frame we can describe the diffusion in terms of a 2 x 2 tensor:

$$\mathbf{D}' \equiv \begin{pmatrix} D_{\perp} & 0 \\ 0 & D_{//} \end{pmatrix} \qquad (15.22)$$

What is more if we choose the image plane to correspond to the centre of symmetry of the lens, we only require one angle θ to describe the orientation of the principal axis of the diffusion tensor with respect to the gradients g_x and g_z say. Consequently we only require four images to calculate $D_{//}$, $D_{\perp}$ and θ, corresponding to gra-
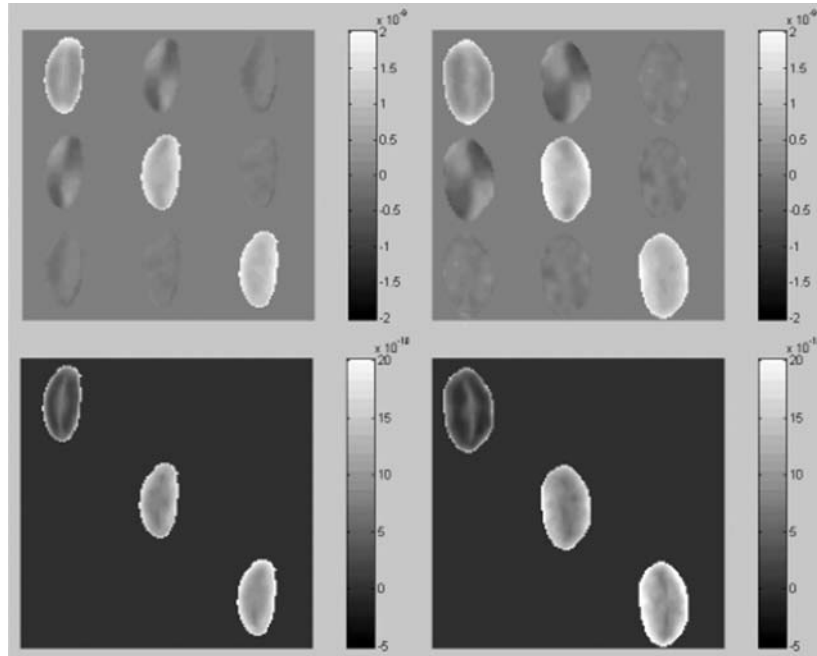
Figure 15.7. Diffusion tensor images of human eye lenses in vitro from a 29 year old donor (left column) and an 86 year old donor (right column) (7). Top row images are of the raw (undiagonalised) diffusion tensor; those in the bottom row are after diagonalisation.

dients of 0, g_x, g_z and $\dfrac{1}{\sqrt{2}}(g_x + g_z)$.

The next problem is how to display the data, since even in this case of cylindrical symmetry and a 2 x 2 diffusion tensor, we have 3 parameters to display for each pixel! The method we have developed using MATLAB is to display for each pixel a pair of orthogonal lines whose lengths are proportional to $D_{//}$ and $D_\perp$ respectively, with the direction of the larger component defining the angle θ viz:
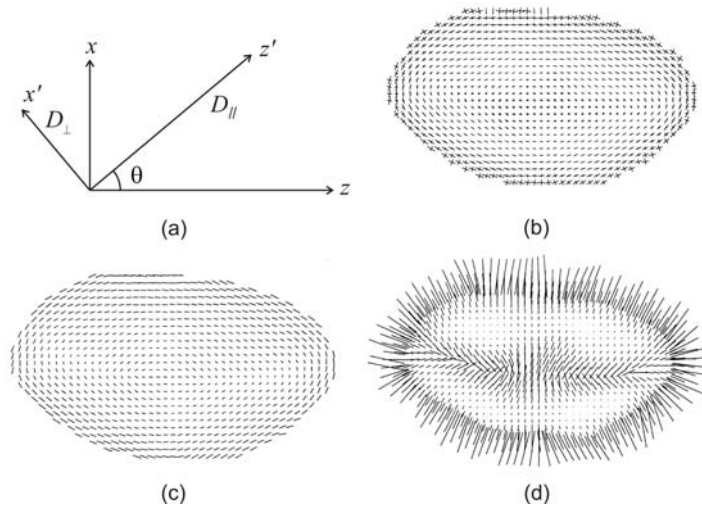
Figure 15.8 2D diffusion tensor images of a human eye lens from a 29 year old donor: a) axes of the principal components $D_{//}$ and $D_{\perp}$ of the diagonalised diffusion tensor with respect to the directions of the diffusion gradients; b) quiver plot showing both principal components on the same scale; c) and d) plots of $D_{//}$ and $D_{\perp}$ respectively.

More generally, if the diffusion tensor does not display cylindrical symmetry, there are 6 parameters to define per pixel (three eigenvalues and three Euler angles defining the directions of the eigenvectors relative to the laboratory frame). In such cases it may be necessary to map the principal eigenvalues, the orientations of the eigenvectors, the fractional anistropy and the mean eigenvalues (see below) as separate diffusion maps or images in order to visualise the full diffusion tensor.

15.2.5 Data Acquisition

In situations where time is limited by the need to minimise motion artefacts or to achieve adequate patient throughput, it may be practical

only to acquire data for the minimum number of diffusion gradient combinations required to define the diffusion tensor. In other cases it may be necessary to employ signal averaging in order to reduce 'sorting bias' (see below) and/or to acquire data for additional gradient directions to improve precision in measuring the eigenvalues and eigenvectors of the diffusion tensor and derived parameters such as the fractional anisotropy (FA). Even for the case where the number of gradient directions is restricted to the minimum value (6), significant improvements in precision of DTI-derived parameters can be achieved by appropriate choice of those directions (8).

Several authors have investigated optimum strategies for measuring diffusion parameters in anisotropic systems using MRI (4,5,8-13). Jones et al. (9) derived expressions for the optimum diffusion weighting (b values) and the optimum ratio of the number of signal acquisitions acquired with high diffusion weighting (N_H) to the number (N_L) with low or minimum diffusion weighting, for which $b \sim 0$. (Note that for an imaging sequence $b = 0$ is generally not strictly achievable due to the influence of the imaging gradients which produce some diffusive attenuation of the signal.) If the effects of transverse relaxation (T_2) are ignored they found $b = 1.09 \times 3/\mathrm{Tr}(D)$ and $N_H = 11.3 \cdot N_L$, where $\mathrm{Tr}(D)=D_{xx}+D_{yy}+D_{zz}$ is the trace of the diffusion tensor and b here refers to the difference in diffusion weighting between high and low values (assuming the latter is non-zero). This result applies provided that the diffusion is not too anisotropic (so that diffusive attenuation is similar in all directions). It compares with the situation of minimum overall imaging time in

which each of the 7 combinations of gradient magnitude and direction is applied only once, for which clearly $N_H = 6N_L$ and according to Jones et al. (9) the optimum $b = 1.05 \cdot 3/\text{Tr}(D)$. However these results must be modified to take account of the effects of T_2 relaxation, which results in additional signal attenuation since it is necessary to operate with a finite echo time TE in order to allow sufficient time to apply the gradients. For example, in the case of white matter in the human brain, for which $T_2 \sim 80$ ms, Jones et al. (9) find that it is necessary to reduce both the b value and the ratio N_H/N_L to ~77% of the asymptotic (long T_2) values quoted above.

Chang et al. (14) used a first order perturbation method to derive analytical expressions for estimating the variance of diffusion eigenvalues and eigenvectors as well as DTI derived quantities such as the trace and fractional anisotropy of the diffusion tensor, for a given experimental design and over a useful range of signal to noise ratios. They also validated their results using Monte Carlo simulations.

A number of authors have compared the merits of applying diffusion gradients in more than the minimum six directions. Some reports (10,12) have suggested there may be no advantage in using more than the minimum number of sampling directions provided that the selected orientations point to the vertices of an icosahedron (11). However a more recent Monte Carlo analysis (5) supports earlier suggestions (13,15) that ~20-30 unique and evenly distributed sampling directions are required for robust estimation of mean

diffusivity, fractional anisotropy (FA) and diffusion tensor orientation. Batchelor et al. (11) conclude that 'the recommended choice of (gradient) directions for a DT-MRI experiment is … the icosohedral set of directions with the highest number of directions achievable in the available time.'

The use of multiple sets of magnetic field gradient directions is of particular importance for applications involving fibre tracking in the brain. Fibre tracking or 'Tractography' is used to infer axonal connectivity in the white matter of the brain (16-19). It relies on the fact that the myelin sheaths surrounding neuronal fibres in the white matter restrict water diffusion perpendicular to the direction of the fibre bundles, while diffusion parallel to the nerve fibres is relatively unrestricted. Consequently the eigenvectors corresponding to the largest eigenvalues reflect the (average) fibre direction within a voxel. By analysing the directions of the principal eigenvectors in adjacent voxels, it is possible to trace the fibre tracts and infer connectivity between different regions of the brain. The situation becomes more complicated if two or more fibre bundles with significantly different directions intersect or cross within a voxel due to partial volume effects. (Typical voxel dimensions in DTI $\sim$ 1-3 mm are much larger than the individual white matter tracts $\sim$ 1- 10μm). Behrens et al. (20) estimate that a third of white matter voxels in the human brain fall into this category. In such cases the use of a single diffusion tensor will yield a principal diffusion eigenvector that represents a weighted average of the individual fibre directions and as such will not correspond to the direction of any of the individual fibre bundles. This

problem can be at least partially alleviated by acquiring data for multiple gradient directions using high angular resolution diffusion imaging (HARDI) and employing spherical tomographic inversion methods (21) or constrained spherical deconvolution (CSD) techniques (22) to model the resulting DWI data in terms of a set of spherical harmonics rather than a single diffusion tensor. High angular resolution diffusion imaging (HARDI) techniques employ stronger diffusion weighting gradients (b-values ≥ 3000 s/mm^2) compared with those ~ 1000 s/mm^2 more routinely employed in clinical DTI. Recently Tournier et al. (23) using such methods have shown in a DWI phantom that it is possible to resolve two fibre orientations with a crossing angle as small as 30°.

15.3 Digital processing of Diffusion-Tensor images

The raw data set obtained from a DTI measurement described in Section 15.2 contains one or more zero-gradient images and six or more diffusion-weighted images corresponding to distinct diffusion directions. In order to render this data in a form amenable to interpretation, the following processing steps are usually performed:

(I) For each voxel in the image, the six independent components of the diffusion tensor (DT) are calculated. The tensor obtained in this step is the so-called *laboratory-frame* DT: it is linked to laboratory-based coordinate axes, which may be defined as the directions of the hardware X, Y, Z gradient coils or the Read, Phase and Slice directions of the image.

(II) The laboratory-frame diffusion tensor can then be diagonalised. The diagonalisation procedure yields:

(i) the principal diffusivities or *eigenvalues* D_1, D_2 and D_3 of the diffusion tensor;

(ii) the orientation of the principal axes or *eigenvectors* of the DT with respect to the laboratory frame.

This represents the DT in the 'sample' frame linked to the physical alignment order in the tissue. The relationship between the laboratory-frame and the diagonalised DT is illustrated in Fig. 15.9 and discussed in detail later in this Section.

Steps (I) and (II) can be regarded as the primary DTI processing. These steps are common to all DTI processing and carried out irrespective of the tissue imaged.
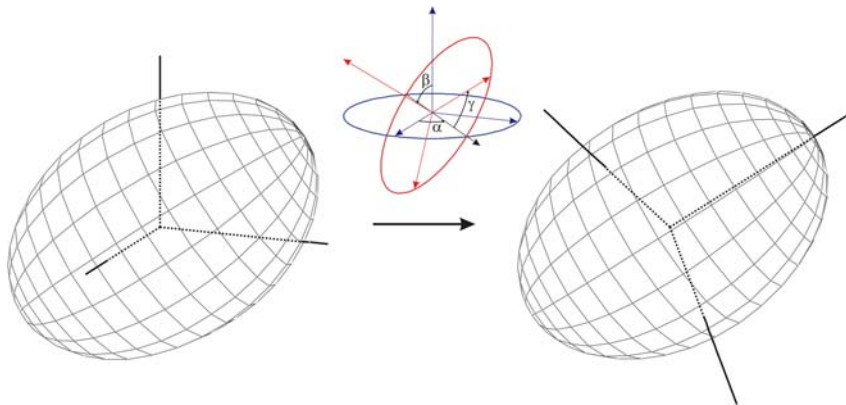

Figure 15.9 Diagonalisation of the diffusion tensor involves finding the rotation of the coordinate frame that aligns the coordinate axes with the principal axes of the ellipsoid.

(III) In "secondary" processing, the diffusion-tensor image obtained in step (II) is represented as a voxel-by-voxel map of one or more of the following parameters:

> direction of the principal eigenvector;
>
> angle between the principal eigenvector and a specified axis;
>
> principal eigenvalue (maximum diffusivity);
>
> mean eigenvalue (mean diffusivity);
>
> fractional anisotropy;
>
> the non-axial anisotropy parameters of the DT.

The user must decide what DT parameters best enable visualisation of the image acquired.

(IV) In "tertiary" processing the information from individual voxels is translated into "global" characteristics describing the image as a whole. An example of such analysis is the nerve fibre tracking used in DTI of the brain or the spinal cord. The voxels of the image are grouped into tracts such that the principal eigenvectors of the voxels within a tract form continuous "flow lines" representing a large bundle of axons.

Unlike the primary DTI processing, the secondary and tertiary processing are organ- or tissue-dependent. The choice of the processing approaches and the DT metrics is determined by the morphology of the tissue and the information sought about the tissue. In avascular tissues, the objective is to characterise the overall alignment order in the tissue rather than identify individual fibres. (The latter is not possible because of the huge number of

fibres within a single voxel). Examples of secondary processing of DT images of cartilage will be presented in Section 15.4.

In the following, we provide an overview of the basic principles and the mathematics underlying DT image processing. The processing techniques are described without reference to a specific platform and are generally applicable.

15.3.1 Primary DTI processing: Calculation of the laboratory-frame diffusion tensor

In Section 15.2, the signal intensity was represented as a function of the diffusion gradient as shown in Eq. (15.20). This representation provides an intuitive and visual explanation of the diffusive atteniuation of the signal in DT images. In practice, it is more convenient to base DTI processing on the so-called **B matrix**. Equation (15.20) can be rewritten as follows (24):

$$\ln\left[\frac{S(\mathbf{g})}{S_0}\right] = -\sum_{i=1}^{3}\sum_{j=1}^{3}b_{ij}D_{ij} \equiv -\mathbf{b}:\mathbf{D} \qquad (15.23)$$

where the indices i, j take the values of x, y or z. The B matrix, $\mathbf{b}$, is a 3 x 3 real symmetric matrix. In the spin-echo experiment, its values are given by

$$b_{ij} = \gamma^2 g_i g_j \delta^2 (\Delta - \delta/3) \qquad (15.24)$$

where g_i, g_j are the components of the diffusion gradient vector $\mathbf{g}$. The B matrix is an extension of the quantity b introduced in Eq. (15.18) to multiple gradient directions.

There are two main advantages to using the B matrix rather than the gradient vectors for processing of DT images. First, the functional form of the signal attenuation is dependent on the DTI pulse sequence used. Equation (15.20) applies to the basic spin-echo pulse-sequence with rectangular diffusion gradients. The attenuation expression is different if a different pulse sequence or non-rectangular diffusion gradients are used (25). Calculation of the attenuation factor can be difficult and time-consuming for the general pulse sequence (26). Fortunately, the attenuation equation is amenable to algorithmic, software-based calculation. When the attenuation factor is kept in the simple and general form given by Eq. (15.23), any pulse sequence-specific factors can be incorporated into the B matrix as part of the algorithm. The software of most modern MRI spectrometers is capable of automatic calculation of the B matrix for any pulse sequence installed on the spectrometer, eliminating the need for the operator to perform this time-consuming calculation manually.

The second advantage of using the B matrix is that it facilitates accounting for contribution to the diffusive attenuation due to the imaging gradients. This source usually leads to much smaller attenuation than the diffusion gradients. However, it can be important when an accurate diffusion tensor is sought or when imaging at high spatial resolution. As with diffusion-gradient attenuation factors, the spectrometer software can automatically build all the pulse sequence-specific corrections to the diffusion attenuation factor into the B matrix. Once the B matrix for each

diffusion gradient is known, the calculation of the diffusion tensor can be performed in a way that is independent of the measurement method. Automatic calculation of the B matrix means that DTI processing is greatly simplified from the operator's point of view.

Equation (15.23) yields the signal attenuation for a known B matrix and a known diffusion tensor. In DTI measurements, where the diffusion tensor is not known *a priori*, the inverse problem must be solved: the diffusion tensor needs to be determined from a set of $N_G \geq 7$ measurements of the signal intensity. In this inverse problem, the inputs are N_G distinct 3 x 3 B matrices (one B matrix for each diffusion gradient vector) and the corresponding N_G measured signal values. The diffusion tensor is the output. In diffusion tensor *imaging*, this problem is solved for each voxel in the image, yielding a separate diffusion tensor for each voxel (see Fig. 15.10).

In practice, two typical scenarios are encountered:

(1) The diffusion gradient directions correspond to the "pure" elements of the laboratory-frame DT: D_{xx}, D_{xy},..., as shown in Eq. (15.21) and Fig. 15.2a.

In this scenario, the diagonal elements of the laboratory-frame diffusion tensor are simply the diffusivities along the respective gradient directions:

$$D_{ii} = -\frac{1}{b} \ln \left(\frac{S_{ii}}{S_0} \right) \qquad i = x, y, z \qquad (15.25)$$

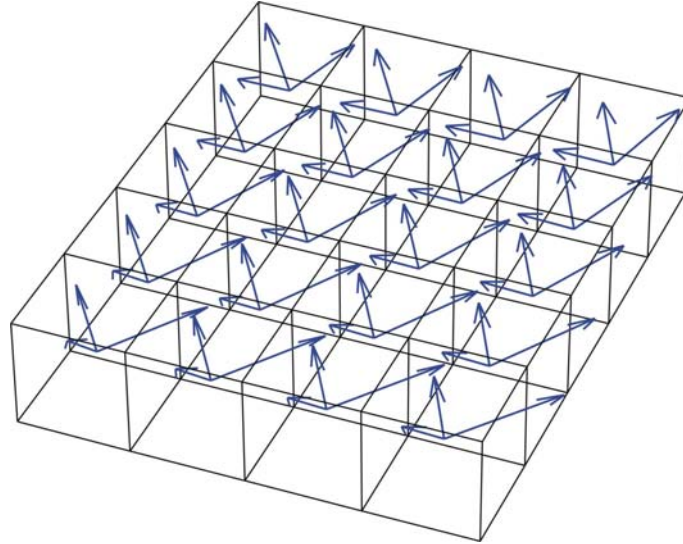The off-diagonal elements are given by (27):

Figure 15.10 Schematic illustration of a DTI dataset. Each voxel in the image is characterised by a unique diffusion tensor: three eigenvalues (the principal diffusivities) and three mutually perpendicular eigenvectors. In this illustration, the lenghts of the eigenvectors are proportional to the corresponding eigenvalues.

$$D_{xy} = -\frac{1}{2b}\left(\ln\frac{S_{xx}}{S_0} + \ln\frac{S_{yy}}{S_0} \right) + \frac{1}{b}\ln\frac{S_{xy}}{S_0}, \text{ etc.} \qquad (15.26)$$

Equations (15.25) and (15.26) are applicable only in the special case when the gradient directions are given by Eq. (15.21). This special case is very instructive for beginners because it visually and simply illustrates the meaning of the diagonal and the off-diagonal elements of the diffusion tensor.

(2) The second scenario is a data set containing more than the minimal number of diffusion gradient directions, as illustrated in Fig. 15.2b.

In this case, the signal corresponding to each direction depends on a combination of several (potentially all) elements of the diffusion tensor. The diffusion tensor is determined using least-squares fitting of Eq. (15.23) to all the measured signal values simultaneously:

i) Create a vector of length N_G containing the signal values from the N_G measurements: $\mathbf{s} = (S_1 \ldots S_{NG})$.

ii) For each $n = 1 \ldots N_G$, calculate $y_n = -\ln(S_n)$;

iii) Set up the linearised least-squares fit equation:

$$y_n = A + \sum_{i=1}^{3}\sum_{j=1}^{3}\left(b_{ij}\right)_n D_{ij} \qquad (15.27)$$

Because the matrix $\mathbf{D}$ in Eq. (15.27) is symmetric ($D_{ij} \equiv D_{ji}$), the LSF involves 7 parameters: 6 independent elements of the symmetric DT and the 7th is the amplitude of the non-attenuated signal.

iv) Find the set of D_{ij} that minimises the sum of the squared differences between s_n and y_n. This can be done using the standard linear LSF procedure (28) or mathematical software packages such as *Mathematica* or Matlab. The elements D_{ij} comprise the reconstructed laboratory-frame diffusion tensor.

The LSF-based approach of scenario (2) is generally applicable: it can be used with an arbitrary pattern of the gradient directions (including the optimal-sampling patterns discussed in Sec. 15.2) as well as the minimal 6+1 dataset. The zero-gradient measurement S_0 is crucially important in both scenarios. However, in the LSF-based approach the zero-gradient measurements do not have a special status: the least-squares fitting procedure treats them on par with diffusion-attenuated points. Nevertheless, the importance of the zero-gradient measurements can be recognised by assigning a greater LSF weight to them than to diffusion-attenuated measurements.

As discussed earlier, one advantage of the LSF-based approach is that it allows the diffusive attenuation due to imaging gradients to be accounted for easily. Its other advantage is that, when redundant measurements are available (i.e., when more than the minimal set of 6+1 measurements was made), it enables an estimation of the standard errors of the DT elements. This can be done as part of the LSF and does not require additional computation time. In the absence of redundant measurements, the seven parameters can always be adjusted to fit the 7 "minimal" measurements exactly; therefore, this advantage is realised only when redundant measurements are available.

15.3.2 Diagonalisation of the diffusion tensor

The laboratory-frame diffusion tensor is difficult to interpret directly because its off-diagonal elements lack a straightforward

physical meaning. The off-diagonal elements can be negative; therefore, they are **not** simply the diffusivities along the directions given by Eq. (15.21) (any diffusivity must be positive).

To enable a physical interpretation, the laboratory-frame DT is usually subjected to diagonalisation. In the first approximation, diagonalisation can be visualiased as a 3D rigid-body rotation that aligns the laboratory-frame coordinate axes with the principal axes of the DT ellipsoid, as shown in Fig. 15.9. Such a rotation is described by the *Euler angles* α, β, γ, which relate the orientation of the principal axes of the DT to the laboratory axes. The lengths of the principal axes correspond to the principal diffusivities (also known as the DT eigenvalues). The directions of the principal axes relative in the laboratory frame are known as the DT eigenvectors. DT eigenvectors tend to represent the alignment order in the tissue and therefore provide a means of visualising the tissue microstructure.

Diagonalisation may also involve permutations of the coordinate axes or inversion of the signs of some or all of the axes. This is because there is no physical distinction between the positive and the negative direction of DT eigenvectors. In general, diagonalisation is represented by a *unitary transformation*:

$$\mathbf{D}' = \mathbf{U}(\alpha,\beta,\gamma)\,\mathbf{D}\,\mathbf{U}^{+}(\alpha,\beta,\gamma) \qquad (15.28)$$

where **U** is a unitary matrix, defined as a matrix whose Hermitian conjugate equals its inverse: $UU^+ = 1$. Rotational transformations illustrated in Fig. 15.9 are a subset of unitary transformations.

In general, a given diffusion tensor can be diagonalised by more than one matrix **U**. **U** can be found using the standard algorithms such as Jacobi diagonalisation (28). Packages such as *Mathematica* or Matlab contain built-in diagonalisation functions that can be used for this purpose.

A general property of unitary transformations is that they conserve the sum of the diagonal elements (the *trace* of the matrix). Therefore, the trace of the DT remains unchanged under a transformation given by Eq. (15.28). This means that the mean diffusivity can be found from the laboratory-frame DT without diagonalisation:

$$D_{av} = \frac{1}{3}\left(D_1 + D_2 + D_3\right) = \frac{1}{3}\left(D_{xx} + D_{yy} + D_{zz}\right) \qquad (15.29)$$

In the experimental setting, the measured signal inevitably contains a contribution from random noise, which can distort the elements of the DT. In the limit of strong noise, the distortion can be sufficiently large to make some of the diagonal elements or the eigenvalues of the DT negative. In this case, the measurement should be considered unreliable and the DT in the given voxel discarded. Alternatively, the DT can be calculated using an algorithm that enforces its positive-definiteness (29).

15.3.3 Gradient calibration factors

Another important factor from the experimental standpoint is the need for gradient calibration factors. On many NMR spectrometers, diffusion gradient amplitudes are set as percentages of the maximum amplitude; however, the absolute amplitude corresponding to "100%" may differ between the x, y and z gradient coils. In this case, it is useful to introduce unitless calibration factors relating the actual and the nominal amplitude of each gradient:

$$\mathbf{g}^{real} = \begin{pmatrix} g_x^{real} \\ g_y^{real} \\ g_z^{real} \end{pmatrix} = \mathbf{C} \cdot \mathbf{g}^{nom} = \begin{pmatrix} C_x & 0 & 0 \\ 0 & C_y & 0 \\ 0 & 0 & C_z \end{pmatrix} \cdot \begin{pmatrix} g_x^{nom} \\ g_y^{nom} \\ g_z^{nom} \end{pmatrix} \quad (15.30)$$

The gradient calibration matrix, $\mathbf{C}$, can be incorporated into the B matrix: in the coordinate system of the hardware gradients, the actual and the nominal matrices are related as $\mathbf{b}^{real} = \mathbf{C} \cdot \mathbf{b}^{nom} \cdot \mathbf{C}$, where $\mathbf{b}^{nom}$ is calculated from the un-calibrated gradient values. It is important to note that $\mathbf{C}$ is not a unitary matrix – rather, it is a rescaling matrix that scales different b_{ij}'s by the appropriate factors.

In a different coordinate system (say, the RPS coordinates), the B matrix can be re-calibrated according to

$$\mathbf{b'}^{real} = \left(\mathbf{UCU}^+ \right) \cdot \left(\mathbf{Ub}^{nom}\mathbf{U}^+ \right) \cdot \left(\mathbf{UCU}^+ \right) = \mathbf{C'} \cdot \mathbf{b'}^{nom} \cdot \mathbf{C'} \quad (15.31)$$

where the $'$ refers to the RPS coordinates.

An alternative approach is to make use of an isotropic region of the sample, for example the saline surrounding the aniosotropic tissue. In an isotropic region, the diffusion attenuation should depend only on the b value (i.e., the trace of the B matrix) and not on the direction of the diffusion gradient. By comparing the attenuation factors of Eq. (15.17) corresponding to different gradient directions, one can empirically introduce scalar calibration factors for each gradient direction. This approach is often more robust than that given by Eq. (15.31).

15.3.4 Sorting bias

Each eigenvalue of the diffusion tensor is associated with a 3D vector that represents the characteristic direction corresponding to that diffusivity, as illustrated in Fig. 15.10. The greatest eigenvalue and the corresponding eigenvector are referred to as the principal eigenvalue and the principal eigenvector. The second largest diffusivity is referred to as the secondary eigenvalue (secondary eigenvector).

In the experimental context identifying the correct order of the eigenvalues is not completely straightforward because of the presence of noise in the images. Noise leads to the so-called *sorting bias*, which can be understood as follows. Suppose that two voxels, A and B, contain physically identical tissue and are therefore characterised by an identical underlying diffusion tensor, D^{True}, with eigenvalues $D_1^{True} \geq D_2^{True} \geq D_3^{True}$. The apparent diffusion tensor is a combination of the underlying DT and a contribution due to noise:

$$D_{1A} = D_{1A}^{true} + \Delta D_{1A} \qquad D_{1B} = D_{1B}^{true} + \Delta D_{1B}$$
$$D_{2A} = D_{2A}^{true} + \Delta D_{2A} \qquad D_{2B} = D_{2B}^{true} + \Delta D_{2B} \qquad (15.32)$$
$$D_{3A} = D_{3A}^{true} + \Delta D_{3A} \qquad D_{3B} = D_{3B}^{true} + \Delta D_{3B}$$

where ΔD_{1A} ... ΔD_{3B} are contributions from noise. Therefore, although the underlying DT in the two voxels is the same, the experimentally measured tensors in voxels A and B usually differ due to the random nature of the noise contribution. Suppose that, in a particular instance, ΔD_{1A} and ΔD_{2B} are negative, while ΔD_{1B} and ΔD_{2A} are positive. If the noise is sufficiently large, or the DT anisotropy small, the order of the eigenvalues in voxel A may be reversed: $D_{1A} < D_{2A}$ but $D_{1B} > D_{2B}$. If the sorting of the eigenvalues is based only on the magnitude of the diffusivity, then the eigenvalues and the eigenvectors in voxel A will be assigned incorrectly: D_{2A} will be taken as the principal eigenvalue and D_{1A} as the secondary eigenvalue. This sorting bias has two main consequences:

1) It results in an overestimation of the principal eigenvalue and underestimation of the secondary eigenvalue. This happens because the diffusivity-based sorting fails to take into account the possibility of negative ΔD_{1A}, which introduces an inherent bias into the distribution of the eigenvalues;

2) In the example above, the direction of the principal DT eigenvector in voxel A will be off by 90° because the eigenvalues

are mis-identified. Therefore, sorting bias also introduces disjoint voxels in an eigenvector map.

The basic principles of techniques that minimise sorting bias can be understood based on the following idea. If the morphology of the tissue varies slowly from one voxel to another, then it can be assumed that the corresponding eigenvectors in neighbouring voxels should have similar directions. Conversely, in the biased example described above, the apparent principal eigenvectors in voxels A and B would be nearly perpendicular. Therefore, in order to minimise sorting bias, the eigenvalues and eigenvectors need to be treated as pairs, and the sorting of eigenvalues needs to take into account the directions of the corresponding eigenvectors. A number of approaches exist that alleviate (but do not completely eliminate) sorting bias (30).

15.3.5 Fractional anisotropy

For a prolate diffusion tensor $(D_1 > D_2 \approx D_3)$, the fractional anisotropy is defined as

$$
\begin{aligned}
\text{FA} &= \sqrt{\frac{3}{2}} \frac{\sqrt{(D_1 - \bar{D})^2 + (D_2 - \bar{D})^2 + (D_3 - \bar{D})^2}}{\sqrt{D_1^2 + D_2^2 + D_3^2}} \\
&= \frac{1}{\sqrt{2}} \frac{\sqrt{(D_1 - D_2)^2 + (D_2 - D_3)^2 + (D_3 - D_1)^2}}{\sqrt{D_1^2 + D_2^2 + D_3^2}}
\end{aligned}
\tag{15.33}
$$

This definition is appropriate for diffusion between long fibres (such as in articular cartilage) or within fibres (e.g., within nerve

fibre tracts). In the case of extreme anisotropy the FA given by Eq. (15.33) equals 1, while in the perfectly isotropic case FA = 0.

For an oblate diffusion tensor ($D_1 \approx D_2 > D_3$), the appropriate definition of the fractional anisotropy is

$$FA = \sqrt{\frac{2}{3}}\frac{\sqrt{(D_1 - \bar{D})^2 + (D_2 - \bar{D})^2 + (D_3 - \bar{D})^2}}{\sqrt{D_1^2 + D_2^2 + D_3^2}} \qquad (15.34)$$

The FA given by Eq. (15.34) can be used for diffusion between confining planes (e.g., diffusion of water molecules in the aqueous domain of lamellar lipid bilayers) and also has the range between 1 (extreme anisotropy) and 0 (isotropic limit).

The value of fractional anisotropy represents the amount of restriction imposed on diffusional displacement of water molecules by the solid component of the tissue (e.g., collagen fibres or cell walls). The value of FA depends on both the relative volume fraction occupied by the solid domain and the degree of alignment of the fibres or cells. FA is therefore a useful morphological metric of the tissue. Specific examples of the relationship between FA and the morphology of the tissue are presented in Section 15.4.

The theoretical value of the fractional anisotropy (FA) defined according to Eqs. (15.33) and (15.34) in the isotropic case is zero. In practice, the presence of noise in MR signal leads to a positive fractional anisotropy even when the underlying eigenvalues of the true DT are equal. The origin of this is fundamentally the same as

the origin of sorting bias discussed above. If $D_{1A}{}^{true} = D_{2A}{}^{true} = D_{3A}{}^{true}$, the measured eigenvalues D_{1A}, D_{2A} and D_{3A} would almost always be different due to the presence of noise, as shown in Eq. (15.32). By combining Eqs. (15.32) and (15.33), it is easily seen that the measured fractional anisotropy in this case given by

$$FA_{noise} = \sqrt{\frac{3}{2}} \frac{\Delta D}{D} \qquad (15.35)$$

Equation (15.35) represents a "noise" fractional anisotropy that is observed in isotropic parts of the sample such as water or saline surrounding the anisotropic tissue. Its magnitude depends on the conditions of the measurement but typically lies in the range 0.01-0.1 (31-33). Non-zero FA due to noise is also observed in Monte Carlo simulations of the diffusion tensor, where it is inversely proportional to the square root of the ensemble size (28,34). Noise fractional anisotropy should be taken as a baseline when interpreting the values of FA in tissue. In the limit of low noise ($\Delta D/D << 1$), the experimentally measured FA is the sum of the "true" underlying FA (FA_{true}) and the noise contribution given by Eq. (15.35):

$$FA = FA_{true} + FA_{noise} \qquad (15.36)$$

15.3.6 Other anisotropy metrics

The FA definitions of Eq. (15.33) and (15.34) are usually used to characterise axially symmetric tensors (when two of the eigenvalues

are equal or nearly equal to each other). In the asymmetric case, the following model-free parameters can be applied to characterise the DT anisotropy:

$$\eta = \frac{1}{3}\left[D_1 - \frac{(D_2 + D_3)}{2} \right]$$
(15.37)

$$\varepsilon = \frac{D_2 - D_3}{2}$$
(15.38)

In the case of axial symmetry $\varepsilon = 0$.

15.4 **Applications of DTI to articular cartilage**

In Section 15.2.4 we discussed two ways of presenting DT images of the eye lens: maps of individual DT elements and eigenvector maps. In the present Section we focus on another avascular tissue, articular cartilage (31-33). We discuss several types of DTI parameter maps used by us for visualising the diffusion tensor in this tissue. Different types of parameter maps emphasise different aspects of the diffusion tensor, and the choice of the type of map to be used is determined by what characteristics of the tissue microstructure need to be gleaned from the images.

15.4.1 Bovine Articular Cartilage

Figure 15.11 shows a spin echo MR image from a sample of bovine patellar articular cartilage (with bone attached) recorded at a magnetic field strength B_0 of 16.4 T. The sample, immersed in

Fomblin® oil (which gives no ^{1}H NMR signal), was oriented with the normal to the articular surface at 55° to the static magnetic field in order to: (1) optimise the signal-to-noise ratio, and (2) suppress the characteristic banding seen in conventional MR images of articular cartilage and ensure relatively uniform signal intensity throughout the cartilage (31). Diffusion-weighted images were acquired with the minimal set of diffusion gradients using a spin-echo pulse sequence with the following acquisition parameters: echo time, 18 ms; repetition time 700 ms; average b value 1550 s·mm^{-2}; 2 ms diffusion gradients; 12 ms diffusion interval; 10 x 12.8 mm field of view; 50 μm in-plane resolution and 400 μm slice thickness. Two images were acquired without diffusion gradients, one of which is shown in Fig. 15.11. Total acquisition time was 14h 38m.
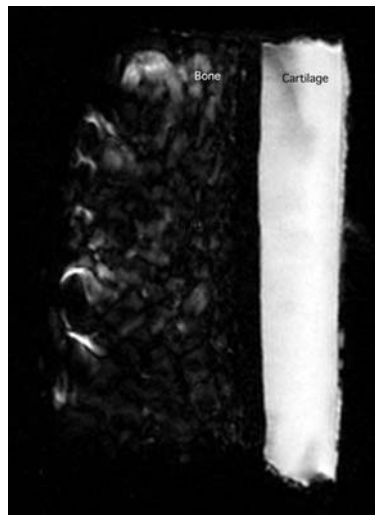
Figure 15.11 A raw SE image of an excised sample of bovine articular cartilage at 16.4 T.
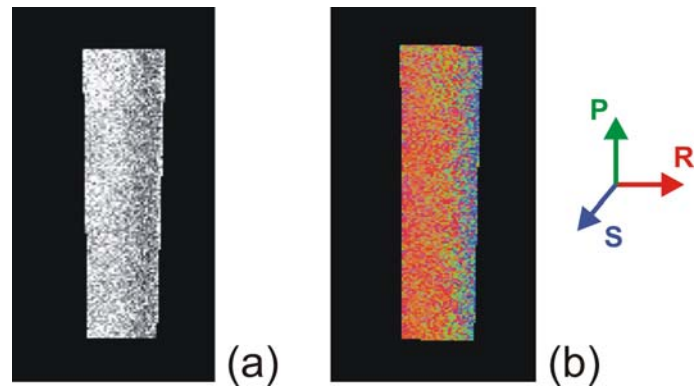
Figure 15.12 (a) Fractional anisotropy map of the sample shown in Fig. 15.11. Black corresponds to FA = 0; white, to FA = 0.15. (b) Directional FA map of the same sample. The colours denote the direction of the principal DT eigenvector: Read, Phase, and Slice gradient directions are shown in red, green and blue, respectively. Colour intensity reflects the magnitude of the FA.
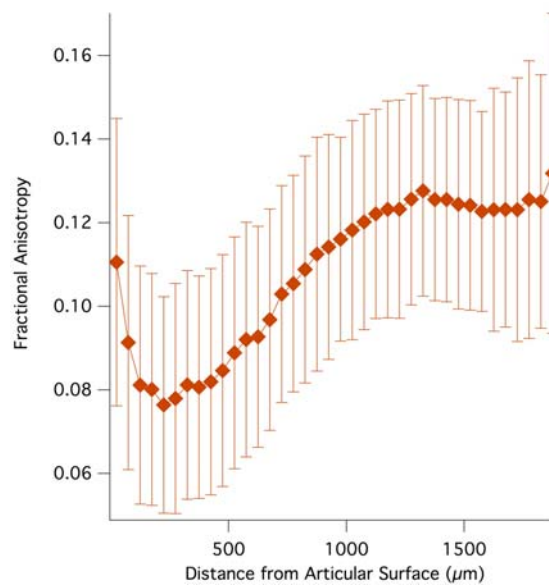

Figure 15.13 The average fractional anisotropy in the same sample plotted as a function of distance from the articular surface.

The magnitude of the fractional anisotropy is shown in Fig. 15.12a with black representing the smallest FA. The direction of the principal diffusion eigenvector within the voxels is incorporated into the map in Fig. 15.12b using colour. Figure 15.13 shows the average FA as a function of distance from the articular surface.

In Fig. 15.14, the principal eigenvectors are scaled by their eigenvalue to enable visualisation of how the collagen fibers 'direct' the diffusion of water perpendicular to the supporting bone in the radial zone. The fibres are less ordered in the transitional zone and align parallel to the articular surface in the superficial zone. This Figure shows the eigenvectors from two contiguous slices.
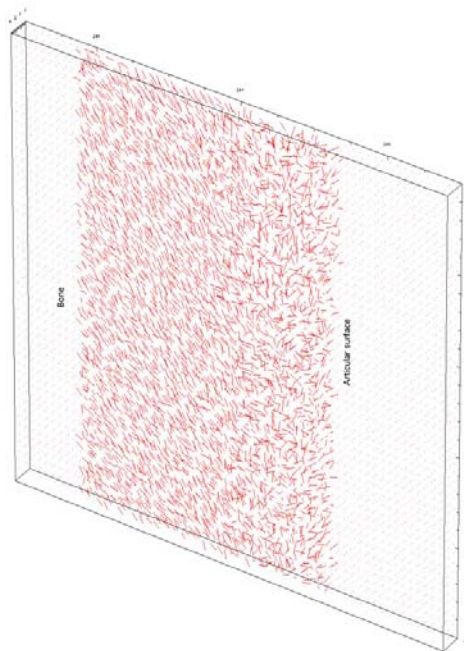
Figure 15.14 A quiver plot showing the directions of the principal DT eigenvectors in the same cartilage sample.

15.4.2 Human Articular Cartilage

The image in Fig. 15.15 was recorded at 7 T from a sample of human right lateral tibia, obtained from a 57-year-old male undergoing complete knee replacement. This region was the only remaining cartilage in the joint and was described by the surgeon as being in poor condition. Acquisition parameters: echo time, 13.3 ms; repetition time 2000 ms; 2 ms diffusion gradient duration; 8 ms diffusion interval; average b value 1075 s·mm^{-2}; 20 x 20mm field of view, with a 156 μm in-plane isotropic voxel dimension and 2 mm slice thickness. Total acquisition time was 19 h.

Figure 15.16 shows the conventional (a) and the directional (b) fractional anisotropy maps for the human cartilage sample shown in Fig. 15.15. The colour coding in the directional map is identical to Fig. 15.12b.
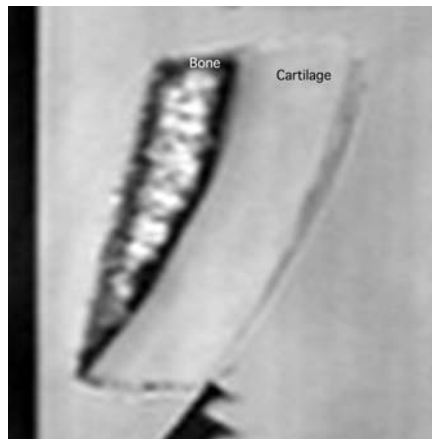
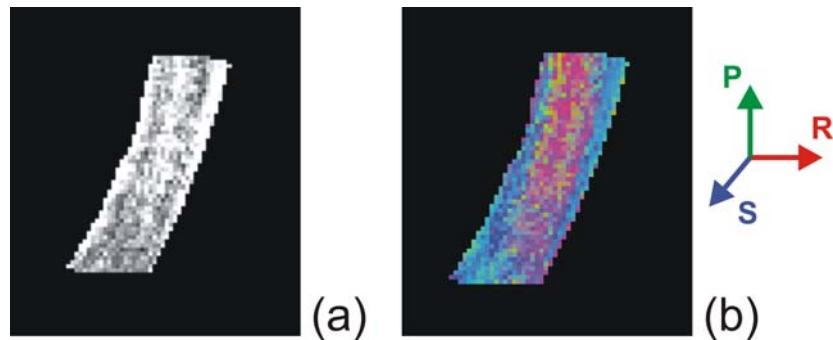**Figure 15.15** MR image of human cartilage recorded at 7 T *in vitro*.

Figure 15.16 The conventional (a) and the directional (b) FA maps of the same human cartilage sample. In (b), the principal eigenvector direction is represented by colours: red, left-right (Read); blue, up-down (Phase); Green, in-out (Slice).
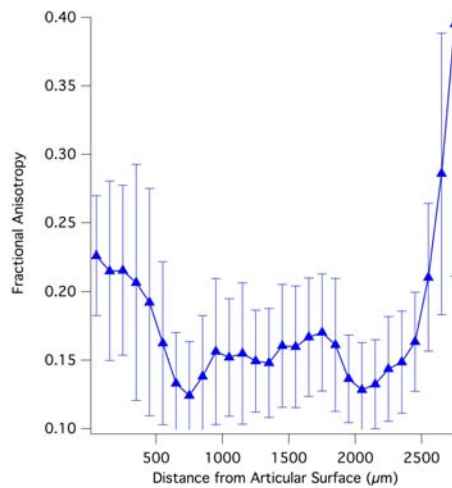

Figure 15.17 The average FA plotted against depth from the articular surface.

The profile of average fractional anisotropy (± std dev) as a function of distance from the articular surface for the human cartilage sample is shown in Figure 15.17. The FA is within the

expected range for cartilage of (0.04-0.28) (33), except for the region near the supporting bone where calcification is likely to contribute to an increase in the observed fractional anisotropy.
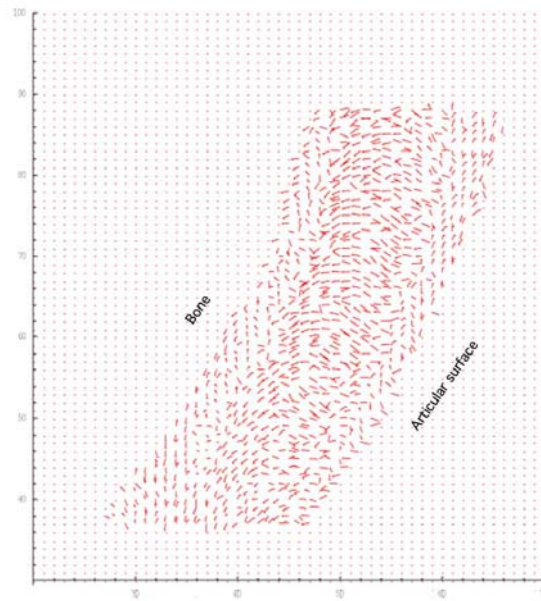

Figure 15.18 Quiver plot showing the principal DT eigenvector for each voxel in the sample.

Figure 15.18 shows a 'quiver' plot for a single slice of the same human cartilage sample in which the principal eigenvector is represented by a line, proportional in length to the principal eigenvalue.

In addition to DTI processing with the Matlab or Mathematica software packages utilised by us, DTI data can be processed using

proprietary software from the scanner manufacturers if available, or transformed data to a common format, such as DICOM, Analyse or NIFTI and processed using one of the readily available shareware diffusion processing packages.

Acknowledgements

References

1.   Einstein A. Zur allgemeinen molekularen Theorie der Wärme. Annalen der Physik 2005;14(S1):154-163.

2.   Tanner JE. Transient diffusion in a system partitioned by permeable barriers. Application to NMR measurements with a pulsed field gradient. J Chem Phys 1978;69(4):1748-1754.

3.   Stejskal EO, Tanner JE. Spin diffusion measurements: Spin echoes in the presence of a time-dependent field gradient. J Chem Phys 1965;42:288-292.

4.   Basser PJ, Jones DK. Diffusion-tensor MRI: theory,

experimental design and data analysis - a technical review. NMR Biomed 2002;15(7-8):456-467.

5.   Jones DK. The effect of gradient sampling schemes on measures derived from diffusion tensor MRI: A Monte Carlo study. Magn Reson Med 2004;51(4):807-815.

6.   Mukherjee P, Chung SW, Berman JI, Hess CP, Henry RG. Diffusion tensor MR imaging and fiber tractography: Technical considerations. Am J Neuroradiol 2008;29(5):843-852.

7.   Moffat BA, Pope JM. Anisotropic water transport in the human eye lens studied by diffusion tensor NMR micro-imaging. Exp Eye Res 2002;74(6):677-687.

8.   Papadakis NG, Xing D, Huang CLH, Hall LD, Carpenter TA. A comparative study of acquisition schemes for diffusion tensor imaging using MRI. J Magn Reson 1999;137(1):67-82.

9.   Jones DK, Horsfield MA, Simmons A. Optimal strategies for measuring diffusion in anisotropic systems by magnetic resonance imaging. Magn Reson Med 1999;42(3):515-525.

10.   Batchelor PG. Optimisation of direction schemes for diffusion tensor imaging. 2002; St Malo, France.

11.   Batchelor PG, Atkinson D, Hill DLG, Calamante F, Connelly A. Anisotropic noise propagation in diffusion tensor MRI sampling schemes. Magn Reson Med 2003;49(6):1143-1151.

12.   Hasan KM, Parker DL, Alexander AL. Comparison of gradient encoding schemes for diffusion-tensor MRI. J Magn Reson Imaging 2001;13(5):769-780.

13.   Papadakis NG, Xing D, Houston GC, Smith JM, Smith MI, James MF, Parsons AA, Huang CLH, Hall LD, Carpenter TA. A study of rotationally invariant and symmetric indices

of diffusion anisotropy. Magn Reson Imaging 1999;17(6):881-892.

14. Chang LC, Koay CG, Pierpaoli C, Basser PJ. Variance of estimated DTI-derived parameters via first-order perturbation methods. Magn Reson Med 2007;57(1):141-149.

15. Skare S, Hedehus M, Moseley ME, Li TQ. Condition number as a measure of noise performance of diffusion tensor data acquisition schemes with MRI. J Magn Reson 2000;147(2):340-352.

16. Poupon C, Mangin JF, Clark CA, Frouin V, Regis J, Le Bihan D, Bloch I. Towards inference of human brain connectivity from MR diffusion tensor data. Med Image Anal 2001;5(1):1-15.

17. Basser PJ, Pajevic S, Pierpaoli C, Duda J, Aldroubi A. In vivo fiber tractography using DT-MRI data. Magn Reson Med 2000;44(4):625-632.

18. Conturo TE, Lori NF, Cull TS, Akbudak E, Snyder AZ, Shimony JS, McKinstry RC, Burton H, Raichle ME. Tracking neuronal fiber pathways in the living human brain. Proc Natl Acad Sci U S A 1999;96(18):10422-10427.

19. Mori S, van Zijl PCM. Fiber tracking: principles and strategies - a technical review. NMR Biomed 2002;15(7-8):468-480.

20. Behrens TEJ, Berg HJ, Jbabdi S, Rushworth MFS, Woolrich MW. Probabilistic diffusion tractography with multiple fibre orientations: What can we gain? Neuroimage 2007;34(1):144-155.

21. Tuch DS. Q-Ball imaging. Magn Reson Med 2004;52(6):1358-1372.

22. Tournier JD, Calamante F, Connelly A. Robust determination of the fibre orientation distribution in diffusion

MRI: Non-negativity constrained super-resolved spherical deconvolution. Neuroimage 2007;35(4):1459-1472.

23. Tournier JD, Yeh CH, Calamante F, Cho KH, Connelly A, Lin CP. Resolving crossing fibres using constrained spherical deconvolution: Validation using diffusion-weighted imaging phantom data. Neuroimage 2008;42(2):617-625.

24. Basser PJ, Mattiello J, LeBihan D. Estimation of the effective self-diffusion tensor from the NMR spin-echo. J Magn Reson B 1994;103(3):247-254.

25. Momot KI, Kuchel PW. PFG NMR diffusion experiments for complex systems. Concepts Magn Reson 2006;28A:249-269.

26. Momot KI, Kuchel PW. Convection-compensating diffusion experiments with phase-sensitive double-quantum filtering. J Magn Reson 2005;174(2):229-236.

27. Coremans J, Luypaert R, Verhelle F, Stadnik T, Osteaux M. A method for myelin fiber orientation mapping using diffusion-weighted MR-images. Magn Reson Imaging 1994;12(3):443-454.

28. Press WH, Teukolsky SA, Vetterling WT, Flannery BP. Numerical Recipes in Fortran. New York: Cambridge University Press; 1992.

29. Lenglet C, Campbell JSW, Descoteaux M, Haro G, Savadjiev P, Wassermann D, Anwander A, Deriche R, Pike GB, Sapiro G, Siddiqi K, Thompson PM. Mathematical methods for diffusion MRI processing. Neuroimage 2009;45(1):S111-S122.

30. Basser PJ, Pajevic S. Statistical artifacts in diffusion tensor MRI (DT-MRI) caused by background noise. Magn Reson Med 2000;44(1):41-50.

31. Meder R, de Visser SK, Bowden JC, Bostrom T, Pope JM.

Diffusion tensor imaging of articular cartilage as a measure of tissue microstructure. Osteoarthr Cartilage 2006;14:875-881.

32.   de Visser SK, Crawford RW, Pope JM. Structural adaptations in compressed articular cartilage measured by diffusion tensor imaging. Osteoarthr Cartilage 2008;16(1):83-89.

33.   de Visser SK, Bowden JC, Wentrup-Byrne E, Rintoul L, Bostrom T, Pope JM, Momot KI. Anisotropy of collagen fibre alignment in bovine cartilage: Comparison of polarised light microscopy and spatially-resolved diffusion-tensor measurements. Osteoarthr Cartilage 2008;16(6):689-697.

34.   Momot KI. Diffusion tensor of water in model articular cartilage. Eur Biophys J 2011;40(1):81-91.